Cancer Imaging

Deutsche Ausgabe: DOI: 10.1002/ange.201507596
Internationale Ausgabe: DOI: 10.1002/anie.201507596

Enzyme-Mediated Modification of Single-Domain Antibodies for Imaging Modalities with Different Characteristics

Mohammad Rashidian[+], Lu Wang[+], Jerre G. Edens, Johanne T. Jacobsen, Intekhab Hossain, Qifan Wang, Gabriel D. Victora, Neil Vasdev, Hidde Ploegh,* and Steven H. Liang**

Abstract: *Antibodies are currently the fastest-growing class of therapeutics. Although naked antibodies have proven valuable as pharmaceutical agents, they have some limitations, such as low tissue penetration and a long circulatory half-life. They have been conjugated to toxic payloads, PEGs, or radioisotopes to increase and optimize their therapeutic efficacy. Although nonspecific conjugation is suitable for most in vitro applications, it has become evident that site specifically modified antibodies may have advantages for in vivo applications. Herein we describe a novel approach in which the antibody fragment is tagged with two handles: one for the introduction of a fluorophore or ^{18}F isotope, and the second for further modification of the fragment with a PEG moiety or a second antibody fragment to tune its circulatory half-life or its avidity. Such constructs, which recognize Class II MHC products and CD11b, showed high avidity and specificity. They were used to image cancers and could detect small tumors.*

The success of immunotherapies, such as the application of monoclonal antibodies against the immune checkpoint inhibitors CTLA4 and PD-1 on T cells and PD-L1 on their targets cannot be viewed separately from the contributions of myeloid cells, which are often present at the tumor margin, and express Class II MHC and/or CD11b products. Macrophages can affect tumor growth by establishing either a detrimental or a favorable microenvironment. Thus, the ability to image myeloid cells' presence is of diagnostic relevance and, compared to tumor-specific markers,[1] may be a more generally applicable approach for detection of tumor cells.[2,3] A commonly used minimally invasive clinical diagnostic approach is the use of 2-[^{18}F]fluoro-2-deoxy-D-glucose positron emission tomography (FDG-PET), which distinguishes areas of high metabolic activity, such as tumors, from surrounding tissue with lesser glucose uptake.[4] These methods do not usually provide information on immune cells in the tumor microenvironment. There are now tools to track immune cells, by the use of isotopically labeled anti-CD11b, anti-Class-II-MHC, and anti-CD8 antibody fragments.[5–7]

The comparatively large size of intact full-sized antibodies results in a long circulatory half-life, and may also hinder efficient tissue penetration.[8] These considerations have driven the search for smaller antibody-derived formats as alternative imaging tools.[1,6] We generated camelid single-domain antibody fragments (VHHs) as the smallest antigen-binding derivatives obtainable from naturally occurring antibodies.[9] VHHs lend themselves to enzymatic modification and have been used in a variety of applications, including imaging.[10]

The relationship between the affinity and valency of the antibodies or their fragments, and their suitability for various imaging applications has received scant attention.[1,11] The production of bivalent single-domain antibodies based on their monovalent equivalents could address issues of avidity, while retaining desirable properties, such as small size. For example, the bivalent derivatives of single-domain antibodies might still be small enough to penetrate tissues, be rapidly cleared from the circulation, yet benefit from increased avidity. On the other hand, tuning of the circulatory half-life could improve the efficiency with which VHHs stain their targets. The attachment of small PEG groups could be used as a tool to "tune" the persistence of a VHH in the circulation. Moreover, PEGylation can decrease the immunogenicity of VHHs, which is important in cases in which repeated administration is required; however, in rare cases even the PEG functionality itself has been suggested to be immunogenic.[12]

Structures of VHHs show that their C terminus is positioned away from the antigen-binding site.[13] We therefore chose a chemical approach to link two fully functional VHHs through their C termini to ensure that their antigen-binding capacity would not be compromised by modification of one of the N termini in the resulting fusion, and that the two binding sites thus created would be truly equivalent, which would be more difficult to ascertain for genetic fusions.

Four sortase substrates were designed and synthesized for the production of dimers or PEGylated VHHs (Figure 1). The substrates either contained two bioorthogonal handles or a handle and a fluorophore. An Alexa647-labeled substrate, **2**, was designed in such a way that the reaction products could be used in fluorescence-activated cell sorting (FACS) experi-

[*] Dr. M. Rashidian,[+] J. G. Edens, Dr. J. T. Jacobsen, I. Hossain, Dr. G. D. Victora, Prof. Dr. H. Ploegh
Whitehead Institute for Biomedical Research
Cambridge, MA 02142 (USA)
E-mail: ploegh@wi.mit.edu

L. Wang,[+] Q. Wang, Prof. Dr. N. Vasdev, Prof. Dr. S. H. Liang
Division of Nuclear Medicine and Molecular Imaging
Massachusetts General Hospital and
Department of Radiology, Harvard Medical School
Boston, MA 02114 (USA)
E-mail: vasdev.neil@mgh.harvard.edu
liang.steven@mgh.harvard.edu

Prof. Dr. H. Ploegh
Department of Biology, Massachusetts Institute of Technology
Cambridge, MA 02142 (USA)

[+] These authors contributed equally.

Supporting information for this article is available on the WWW under http://dx.doi.org/10.1002/anie.201507596.

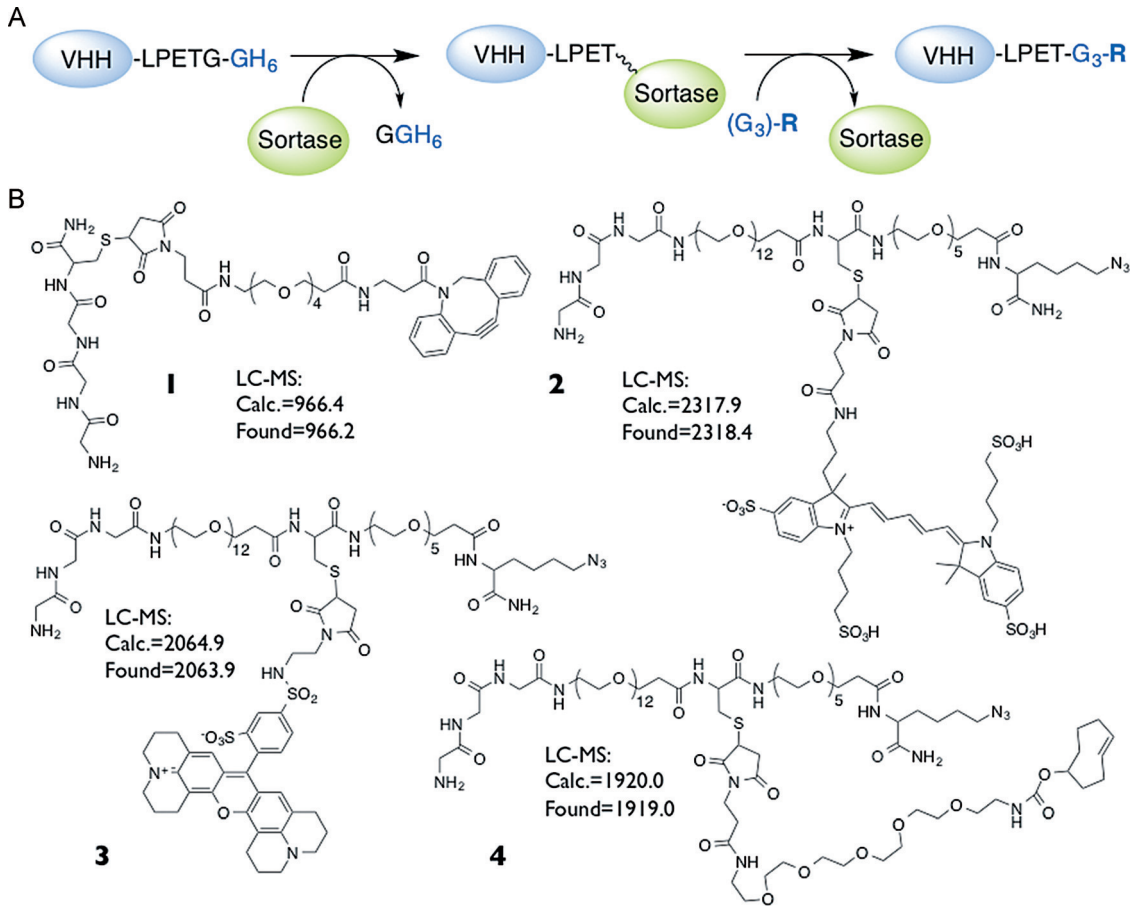

Figure 1. A) Site-specific labeling of VHHs with sortase, which recognizes the "LPXTG" motif and replaces the G residue with a substrate containing a NH_2-G_3 moiety. B) Structures of the substrates containing bioorthogonal functionalities. The structures were confirmed by LC–MS.

ments to estimate relative in vitro binding affinities; a substrate modified with Texas Red, **3**, was designed to enable two-photon microscopy and the estimation of relative in vivo binding affinities; and a *trans*-cyclooctene-modified substrate, **4**, was produced to enable rapid installation of a ^{18}F-labeled-tetrazine radioactive tag for positron emission tomography (PET; ^{18}F $t_{1/2} < 2$ h). The dimers were produced accordingly (Figure 2; see also the Supporting Information).

For DC8 (anti-Class-II), splenocytes were stained with different concentrations of monomers and dimers and analyzed by FACS. For DC13 (anti-CD11b), the CD11b$^+$ mutuDC dendritic cell line was used. For Class II MHC and CD11b, the VHH dimers were found to bind approximately 3.3- and 2.3-fold more strongly than the corresponding monomers, respectively (Figure 3).

We next evaluated the in vivo binding characteristics of the VHH dimers versus monomers. Due to the more abundant expression of Class II MHC molecules on splenocytes as compared to that of CD11b, we explored the in vivo binding affinity of anti-Class-II dimers. Mice were injected intravenously (i.v.) with equal amounts of monomers and dimers (0.25 nmol) of DC8. The mice were euthanized 2 h postinjection (p.i.), and lymphoid organs were excised for examination. The monomers and dimers yielded different staining patterns (Figure 3 B). The dimer showed interspersed yet more pronounced staining than the monomer, thus corroborating the FACS results.

To render monomers and dimers suitable for immuno-PET, we produced dimer VHHs by using substrate **4**. To produce the ^{18}F-labeled tetrazine, we applied a method that was automated in its key steps to minimize operator radiation exposure in the course of preparation (Figure 4 A; see the Supporting Information). Next, we produced ^{18}F-labeled anti-Class-II and anti-CD11b dimers and used them for PET imaging (Figure 4). PET showed that both dimers stained lymphoid organs (Figure 4; see also movies 1 and 2 in the Supporting Information). The anti-Class-II-MHC dimer showed stronger staining of lymphoid organs, particularly the spleen, as compared to the anti-CD11b dimer (Figure 4 D,F). We attribute this behavior to the fact that in the spleen there are fewer CD11b$^+$ cells than Class II MHC$^+$ cells, and less CD11b expressed per cell. We established specificity by blocking the targets of these VHHs by the introduction of unlabeled VHHs as competitors prior to imaging. PET imaging conducted 2 h after the injection of ^{18}F-labeled VHHs showed effective blocking of the signals in the lymphoid organs, thus further underlining the specificity of the signals (Figure 5 C; see also movies 3–6). To further

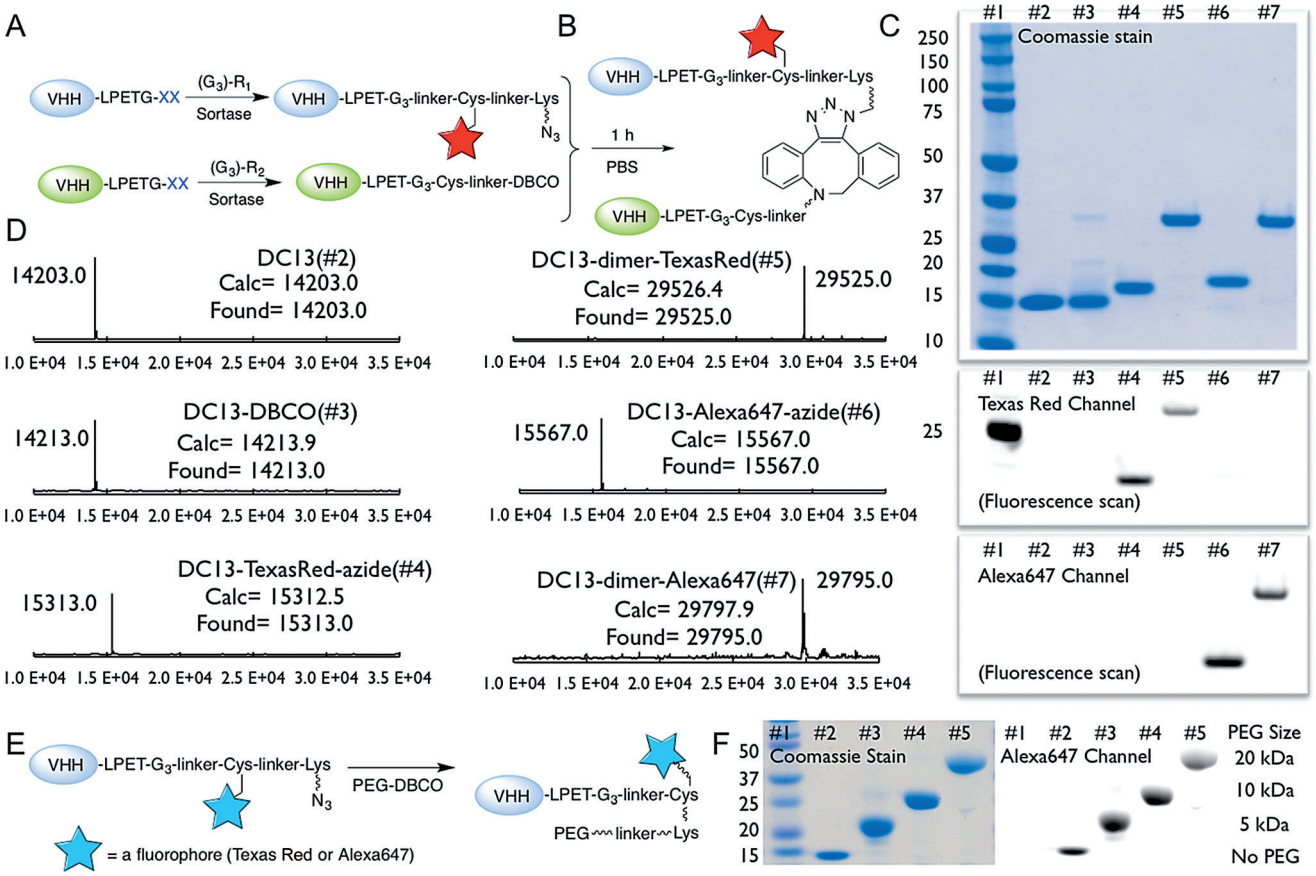

Figure 2. A,B) Synthesis of VHH derivatives. C,D) Characterization of the products. The LC–MS and SDS-PAGE analysis for DC13 is shown (see the Supporting Information for DC8). Lane 1 in (C): marker, lane 2: DC13, lane 3: DC13–DBCO, lane 4: DC13–azide–Texas Red, lane 5: DC13–dimer–Texas Red, lane 6: DC13–N_3–Alexa647, lane 7: DC13–dimer–Alexa647. E,F) PEGylation of VHHs and characterization. Lane 1 in (F): marker, lane 2: DC8–Alexa647–N_3, lane 3: DC8–Alexa647–PEG (5 kDa), lane 4: DC8–Alexa647–PEG (10 kDa), lane 5: DC8–Alexa647–PEG (20 kDa). All materials were purified by size exclusion chromatography. DBCO = dibenzocyclooctyne.

confirm the specificity of the dimers in the absence of competing VHHs, we imaged MHC $II^{-/-}$ and $CD11b^{-/-}$ mice. We detected no PET signals in lymphoid organs, thus further confirming the specificity of both dimers (Figure 4E,G; see also movies 7 and 8).

The monomers and dimers did not differ in uptake into the kidneys and intestine, organs commonly targeted non-specifically by VHHs in the course of their clearance.[14] These experiments helped us set the stage to explore the ability of VHH dimers to image tumors. We imaged two types of tumors with the developed bivalent VHHs by the engraftment of mice with the B16 melanoma or the pancreatic tumor cell line panc02. Both dimers readily detected the lymphoid organs as well as the B16 melanoma tumor (see movies 9 and 10) or the panc02 graft (see movies 11 and 12). Upon excision, the panc tumors were no more than about 1–2 mm in diameter, thus showing the method to be sensitive. Post-mortem biodistribution analysis also correlated well with the FACS and two-photon results (Figure 5A,B). Although the dimers stained secondary lymphoid organs more efficiently than their corresponding monomers, specifically for the anti-class-II-MHC VHH, the PET signals in the tumors showed no commensurate increase (Figure 5A,B). We attribute this observation to the larger size of the dimer as compared to the monomer, which may result in lower penetration in tumors, thus counteracting the effect of the higher affinity of the dimer.

We examined whether we could manipulate circulatory half-life to further improve the signal-to-noise ratio. PEGylation of VHHs results in increased circulatory half-life, and the increase correlates with the size of the attached PEG group.[15] VHHs sortagged with substrate **2** or **3** were treated with DBCO-functionalized PEG (5, 10, or 20 kDa) to yield the final PEGylated VHHs (Figure 2E,F). B6 mice received 5 μg of PEGylated VHH and were euthanized 3 h later, followed by dissection of the lymph nodes and spleen for FACS and two-photon microscopy. FACS showed a significant increase in staining of the PEGylated DC8–Alexa647 versus the non-PEGylated DC8. We observed an approximately 30, 100, and 220% increase in staining for 5, 10, and 20 kDa PEG-conjugated DC8, respectively, thus establishing a correlation between the size of the attached PEG moiety and staining efficiency (Figure 3D). When we injected DC8–Alexa647–PEG (20 kDa), which showed the strongest binding in vivo,

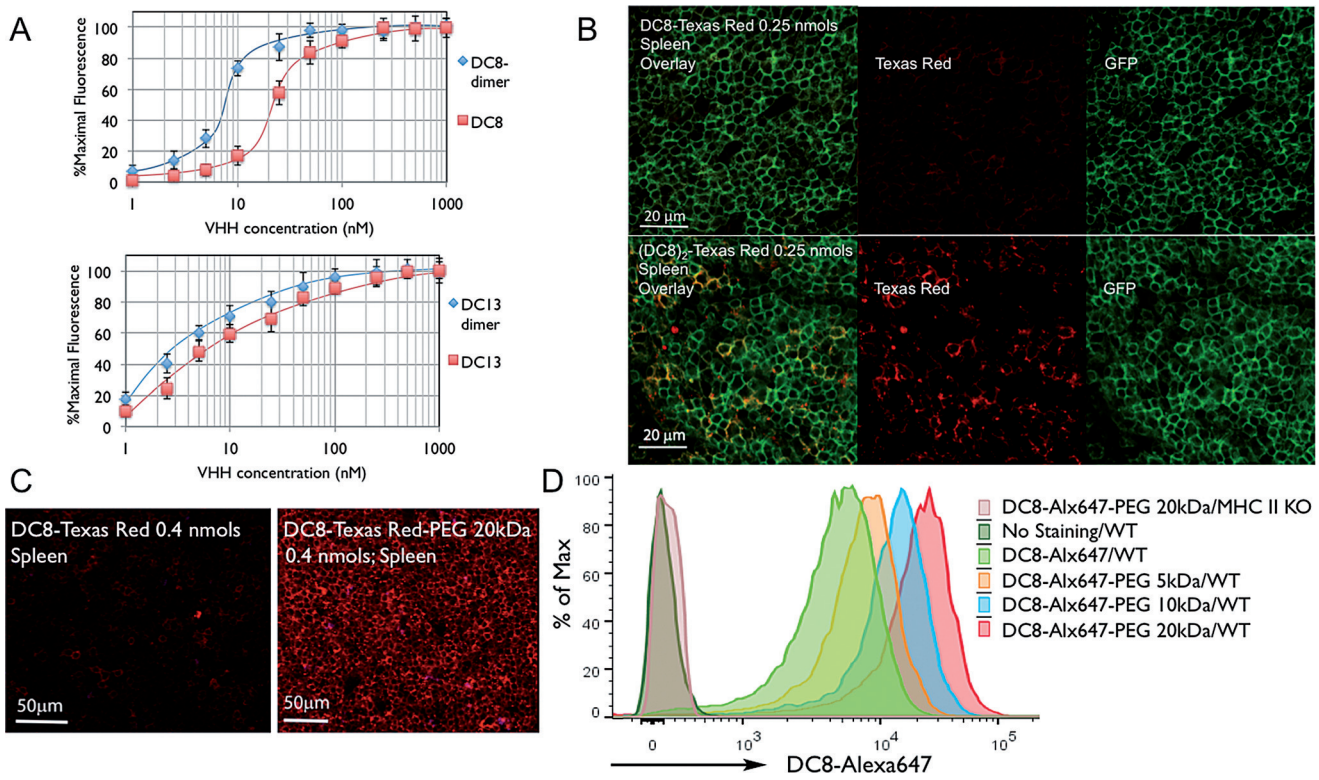

Figure 3. A,B) Dimers were able to stain their targets with increased efficiency as compared to the corresponding monomers. A) Cells were stained in vitro with the indicated concentrations of Alexa647-labeled VHH monomers or dimers. B) Equal amounts of the DC8 monomer and DC8 dimer were injected i.v.; the mice were euthanized 2 h p.i., and their spleens were excised for two-photon imaging. C) Equal amounts of DC8 with or without PEG, both equipped with TexasRed were injected i.v. into mice; spleens were excised 3 h p.i. for two-photon imaging. D) Equal amounts of DC8 with or without PEG, all equipped with Alexa647, were injected i.v. into mice; spleens were excised 3 h p.i., and cells were harvested and analyzed by FACS. WT = wild type.

into a MHC II$^{-/-}$ mouse, FACS analysis showed no staining in the spleen (Figure 3D). This result confirmed that PEGylation does not affect the specificity of the VHHs.

We then explored the PEGylated VHHs for their suitability for PET imaging. VHH DC8 was PEGylated and modified with an ^{18}F radionuclide. PEGylated VHHs showed increased staining of the lymphoid organs, as confirmed by FACS and two-photon microscopy (Figure 5D). The longer circulatory half-life of PEGylated VHHs presumably increases the likelihood of a VHH binding to its target, as long as target accessibility is not compromised by PEGylation. As expected, the ^{18}F-labeled DC8–PEG (20 kDa) had the highest PET signal in blood at the time of imaging (3 h p.i.; Figure 5D). Although the larger 20 kDa PEG can significantly increase the staining efficiency in lymphoid organs, it delays circulatory clearance, a factor to consider when isotopes with short half-lives, such as ^{18}F or ^{11}C, are being used. However, VHHs modified with 10 or 5 kDa PEG still show significantly increased staining efficiency and yet can be rapidly cleared. When isotopes with longer half-lives, such as ^{89}Zr or ^{64}Cu, are used to label VHHs, the use of a 20 kDa PEG moiety should improve staining.

In summary, we have developed a method to produce site specifically PEGylated or bivalent single-domain antibodies equipped with either a fluorophore or radionuclide (^{18}F) for different imaging modalities. The reaction conditions enable full retention of the biological activity of the fusion partners. By cytofluorimetry, dimers bind approximately 3 times more avidly to their targets. Two-photon microscopy confirmed that bivalent single-domain derivatives labeled with Texas Red bind more efficiently to their targets. PEGylated fluorescent VHHs showed improved staining in vivo, with larger PEG substituents giving stronger signals in FACS. In immuno-PET experiments, bivalent ^{18}F-labeled VHHs stained lymphoid organs in vivo more effectively than monomers. ^{18}F-labeled PEGylated VHHs showed improved staining, whereby PEG substituents with a higher molecular weight gave stronger signals. Finally, immuno-PET of two different models of tumor-bearing mice showed that the DC8 dimer and DC13 dimer detected not only lymphoid organs, as expected, but also showed the location of ectopic melanoma and pancreatic tumor grafts. Overall, this study provides further support for the notion that derivatives of single-domain antibodies are a valuable addition to the available imaging and radiodiagnostic toolbox.

Acknowledgements

M.R. is a Cancer Research Institute Irvington Fellow supported by the Cancer Research Institute. S.H.L. is the recipient of an NIH Career Development Award. This

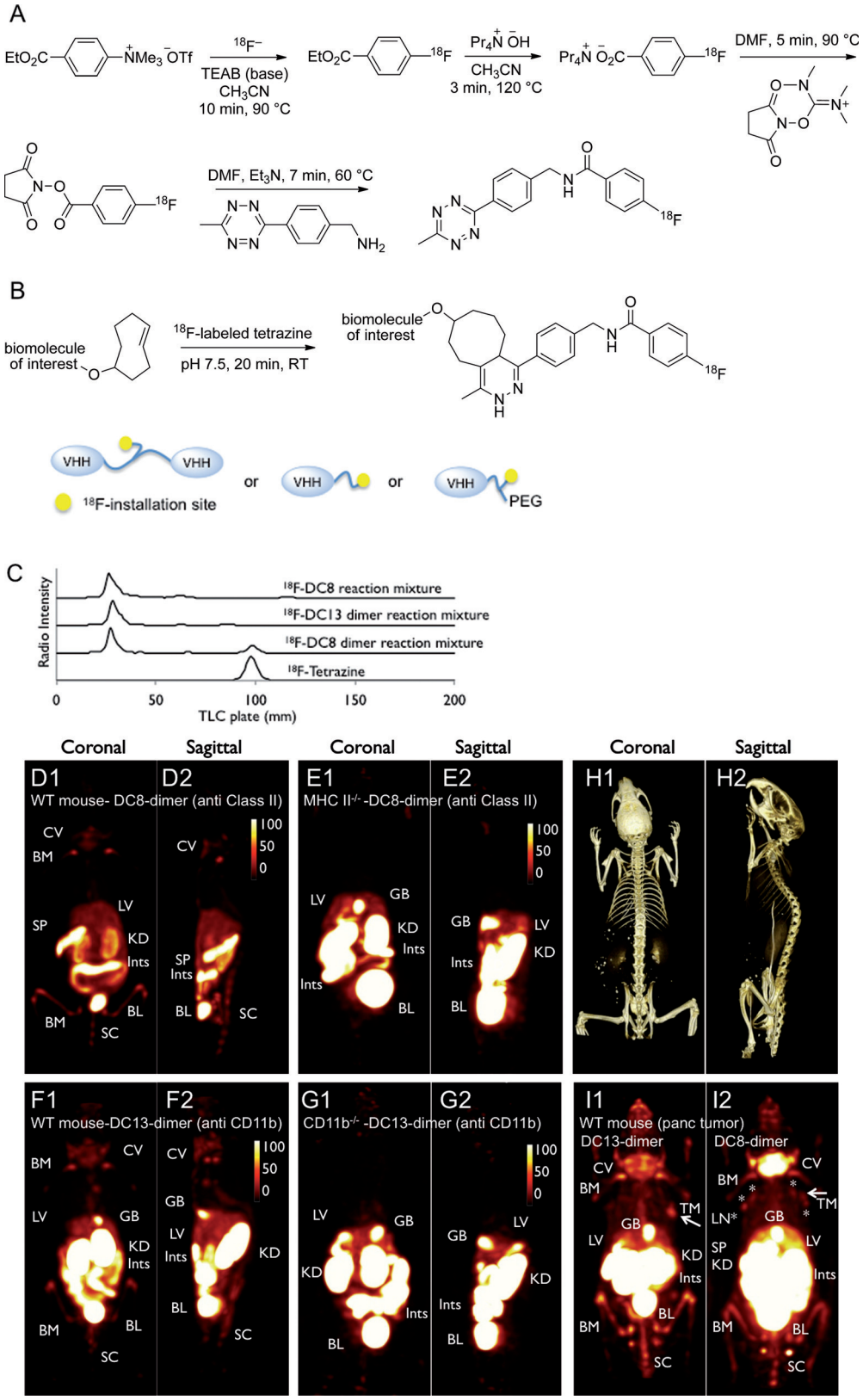

Figure 4. A) Synthesis of an ^{18}F-labeled tetrazine. DMF = *N*,*N*-dimethylformamide, TEAB = triethylammonium bicarbonate. B) ^{18}F labeling of VHH-dimers, VHH monomers, and PEG-functionalized VHHs. C) Radio-TLC analysis of the ^{18}F-labeling reactions. D–I) Use of the ^{18}F-DC8 dimer and ^{18}F-DC13 dimer to detect lymphoid organs and reveal tumors. PET images are shown in both coronal and sagittal views for better visualization. CT images are provided for better visualization (H1,2). D,E) PET images of WT (D) and class II MHC$^{-/-}$ mice (E) 2 h after injection of the ^{18}F-DC8 dimer (see movies S1 and S7 for a 3D visualization). CV: cervical lymph nodes, BM: bone marrow, SP: spleen, GB: gallbladder, LV: liver, KD: kidneys, Ints: intestines, BL: bladder, SC: spinal cord. F,G) PET images of WT (F) and CD11b$^{-/-}$ mice (G) 2 h after injection of the ^{18}F-DC13 dimer (see movies S2 and S8 for a 3D visualization). I1,2) Tumor-associated CD11b+ cells (I1) or class II MHC+ cells (I2) were visualized by using the ^{18}F-DC13 dimer (I1) or the ^{18}F-DC8 dimer (I2). Arrows point at the tumors. In (I2), stars show the lymph nodes (see movies S11 and S12 for a 3D visualization). PET scale bars have arbitrary units. Images are representative for 2–4 mice with similar results.

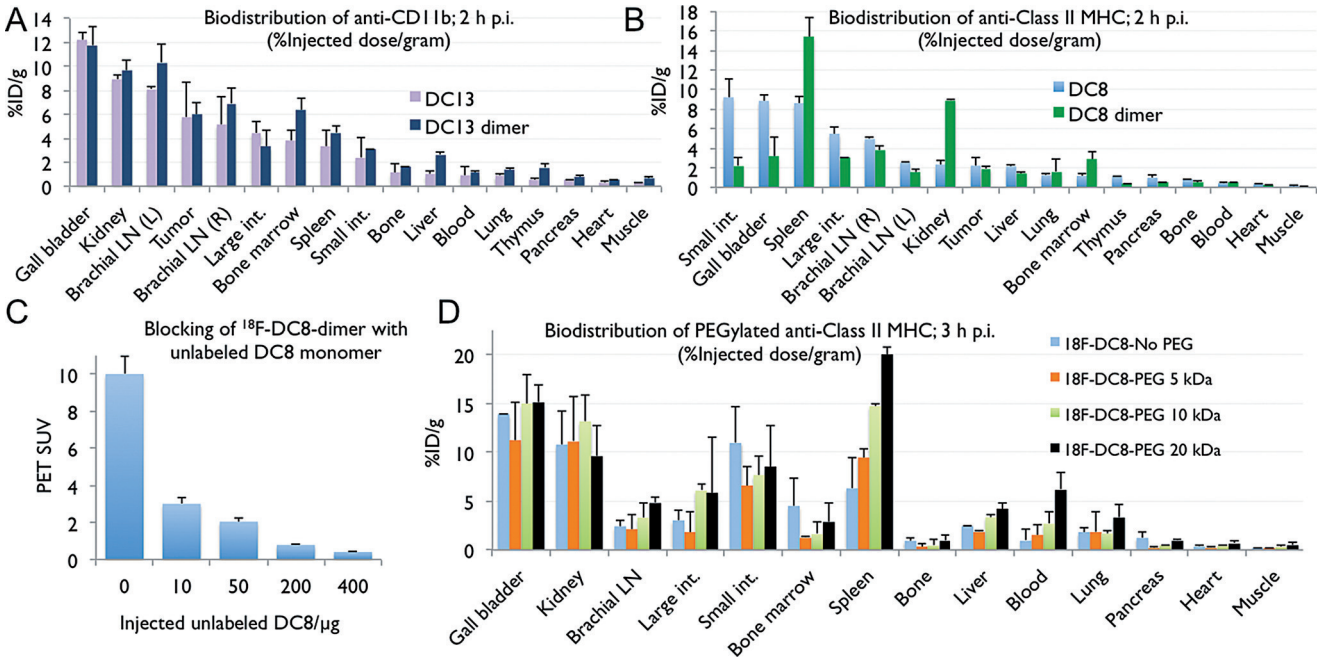

Figure 5. A,B) Postmortem biodistribution of ^{18}F-VHHs in all organs. Mice were injected with the same amount of either ^{18}F-VHH or the ^{18}F-VHH dimer. The activity in different organs was measured 3 h p.i. C) The VHH monomer can block binding of the ^{18}F-VHH dimer. WT mice were injected with different amounts of unlabeled DC8, and the ^{18}F-DC8 dimer was injected 20 min later (50 µCi/5 µg). PET standardized uptake values (SUVs) for spleen were calculated on the basis of PET images acquired 2 h after injection of the ^{18}F-labeled DC8 dimer (see movies S3–S6 for a 3D visualization). D) WT mice were injected with the same amount of different ^{18}F-DC8 derivatives with or without PEG moieties as indicated. The activity in different organs was measured 3 h p.i. (see movies S13–S16 for a 3D visualization). LN = lymph nodes.

research was funded by NIH R01-AI087879-06 (to H.L.P.), DP1-GM106409-03 (an NIH Pioneer Award to H.L.P.), and R01-GM100518-04 (to H.L.P.), and by the Lustgarten Foundation (H.L.P.).

Keywords: enzymes · isotopic labeling · PEGylation · positron emission tomography · single-domain antibodies

How to cite: *Angew. Chem. Int. Ed.* **2016**, *55*, 528–533
Angew. Chem. **2016**, *128*, 538–543

[1] T. Olafsen, S. J. Sirk, S. Olma, C. K.-F. Shen, A. M. Wu, *Tumor Biol.* **2012**, *33*, 669–677.
[2] E. J. Lipson, W. H. Sharfman, C. G. Drake, I. Wollner, J. M. Taube, R. A. Anders, H. Xu, S. Yao, A. Pons, L. Chen, D. M. Pardoll, J. R. Brahmer, S. L. Topalian, *Clin. Cancer Res. Off. J. Am. Assoc. Cancer Res.* **2013**, *19*, 462–468.
[3] T. R. Simpson, F. Li, W. Montalvo-Ortiz, M. A. Sepulveda, K. Bergerhoff, F. Arce, C. Roddie, J. Y. Henry, H. Yagita, J. D. Wolchok, K. S. Peggs, J. V. Ravetch, J. P. Allison, S. A. Quezada, *J. Exp. Med.* **2013**, *210*, 1695–1710.
[4] R. Boellaard et al., *Eur. J. Nucl. Med. Mol. Imaging* **2010**, *37*, 181–200.
[5] M. Rashidian, E. J. Keliher, A. M. Bilate, J. N. Duarte, G. R. Wojtkiewicz, J. T. Jacobsen, J. Cragnolini, L. K. Swee, G. D. Victora, R. Weissleder, H. L. Ploegh, *Proc. Natl. Acad. Sci. USA* **2015**, *112*, 6146–6151.
[6] R. Tavare, M. N. McCracken, K. A. Zettlitz, S. M. Knowles, F. B. Salazar, T. Olafsen, O. N. Witte, A. M. Wu, *Proc. Natl. Acad. Sci. USA* **2014**, *111*, 1108–1113.
[7] M. Rashidian, E. J. Keliher, M. Dougan, P. K. Juras, M. Cavallari, G. R. Wojtkiewicz, J. T. Jacobsen, J. G. Edens, J. M. J. Tas, G. Victora, R. Weissleder, H. Ploegh, *ACS Cent. Sci.* **2015**, *1*, 142–147.
[8] E. C. Dijkers, T. H. Oude Munnink, J. G. Kosterink, A. H. Brouwers, P. L. Jager, J. R. de Jong, G. A. van Dongen, C. P. Schröder, M. N. Lub-de Hooge, E. G. de Vries, *Clin. Pharmacol. Ther.* **2010**, *87*, 586–592.
[9] M. Rashidian, E. J. Keliher, A. M. Bilate, J. N. Duarte, G. R. Wojtkiewicz, J. T. Jacobsen, J. Cragnolini, L. K. Swee, G. D. Victora, R. Weissleder, H. L. Ploegh, *Proc. Natl. Acad. Sci. USA* **2015**, *112*, 6146–6151.
[10] T. De Meyer, S. Muyldermans, A. Depicker, *Trends Biotechnol.* **2014**, *32*, 263–270.
[11] P. Holliger, T. Prospero, G. Winter, *Proc. Natl. Acad. Sci. USA* **1993**, *90*, 6444–6448.
[12] H. Schellekens, W. E. Hennink, V. Brinks, *Pharm. Res.* **2013**, *30*, 1729–1734.
[13] E. De Genst, K. Silence, K. Decanniere, K. Conrath, R. Loris, J. Kinne, S. Muyldermans, L. Wyns, *Proc. Natl. Acad. Sci. USA* **2006**, *103*, 4586–4591.
[14] V. Cortez-Retamozo, M. Lauwereys, G. Hassanzadeh, M. Gobert, K. Conrath, S. Muyldermans, P. De Baetselier, H. Revets, *Int. J. Cancer J. Int. Cancer* **2002**, *98*, 456–462.
[15] Y. Vugmeyster, C. A. Entrican, A. P. Joyce, R. F. Lawrence-Henderson, B. A. Leary, C. S. Mahoney, H. K. Patel, S. W. Raso, S. H. Olland, M. Hegen, X. Xu, *Bioconjugate Chem.* **2012**, *23*, 1452–1462.

Received: August 14, 2015
Revised: October 1, 2015
Published online: December 2, 2015

